Check for updates

Received: 12 November 2025 | Revised: 15 May 2026 | Accepted: 28 May 2026

DOI: 10.1002/rpm2.70066

RESEARCH ARTICLE

RESPONSIVE MATERIALS Open Access WILEY

Electrochemical investigation of radical-radical recognition in viologen-based ditopic structures

Ahmad Bachir[1] | **Fabiana Ciocchetti**[1] | **Caterina Baccini**[2] | **Sayed Suliman Shah**[1] | **Andrea Secchi**[2] | **Cristian Pezzato**[3] | **Giulio Ragazzon**[1]

[1]CNRS, Institut de Science et d'Ingénierie Supramoléculaires (ISIS) UMR 7006, University of Strasbourg, Strasbourg, France

[2]Department of Chemistry, Life Sciences and Environmental Sustainability, University of Parma, Parma, Italy

[3]Laboratory for Macromolecular and Organic Chemistry (MOC), Department of Chemical Sciences, University of Padova, Padova, Italy

Correspondence

Giulio Ragazzon.
Email: ragazzon@unistra.fr

Abstract

Radical-radical interactions between viologen derivatives have been pivotal in advancing molecular machines and interlocked architectures, being the subject of numerous studies. Yet, the investigation of multitopic host-guest pairs has been largely overlooked, despite such systems may lead to the formation of extended polymeric structures. Here, we report the synthesis and electrochemical investigation of ditopic molecules bearing either two blue-box macrocycles or two viologen-based guests, connected via a polyethylene glycol spacer. We discovered that both systems undergo intramolecular homodimerization upon reduction, a process not previously described for similar macrocycles. Electrochemical studies indicated that mixtures of hosts and guests comprising such multitopic architectures can assemble to give short-lived non-equilibrium pseudorotaxanes, and offered insights on the relaxation kinetics to the corresponding monomeric states. The studied systems offer guidance to develop mechanically interlocked polymers based on radical-radical interactions.

Keywords

click chemistry, host-guest, radical-radical interactions, supramolecular chemistry, tris-radical complex

1 | INTRODUCTION

Viologen redox chemistry has been extensively investigated, particularly in the context of interlocked molecular architectures.[1,2] The pioneering work of Stoddart and co-workers introduced the so-called "blue box",[3] a host molecule comprising two face-to-face viologen units, which exhibits high affinity for viologen-type guest molecules upon reduction, thanks to radical-radical interactions.[4–7] This key development has enabled significant advances in the field of artificial molecular machines,[8] finding application in switches,[9] molecular pumps,[10–19] and other architectures.[20,21]

Despite substantial progress in the design and functionalization of guest molecules,[7–16,18] structural modifications to the blue box host have been limited, being rarely studied in combination with radical-radical interactions.[22–25] In fact, besides our own recent work,[26] we could identify only a few studies where redox-powered pumping is realized using diverse blue box macrocycles.[27,28] Specifically, Stoddart and co-workers prepared molecule **I**·7PF$_6$ (Figure 1a), which bears at one end a blue-box macrocycle and on the other end a "pump head" composed of 3,5-dimethylpyridinium and bipyridinium units.[27] This structure, comprising both host and guest in the same molecule, can be part of daisy-chain architectures. Upon subsequent reduction and oxidation, the authors used a combination of nuclear magnetic resonance (NMR) techniques to reveal the formation of extended polyrotaxane structures, with an upper bound of 11 molecules assembled.

Ahmad Bachir and Fabiana Ciocchetti contributed equally.

This is an open access article under the terms of the Creative Commons Attribution License, which permits use, distribution and reproduction in any medium, provided the original work is properly cited.

© 2026 The Author(s). *Responsive Materials* published by John Wiley & Sons Australia, Ltd on behalf of Southeast University.

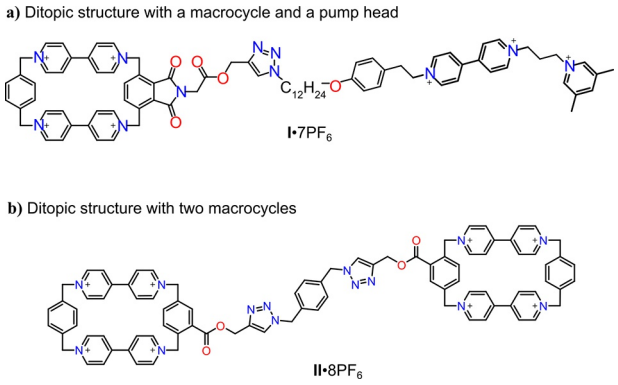


FIGURE 1 State of the art for multitopic viologen structures. (a) Ditopic structure consisting of one macrocycle and one viologen-containing axle, **I**·7PF_6. (b) Ditopic structures consisting of two macrocycles, **II**·8PF_6.

Daisy-chain structures offer the benefit of investigating a single molecule, yet the intrinsic self-complementary position of host and guest in the molecule facilitates the formation of short oligomers, such as dimers and trimers.[20,21] Having linear molecules with either two hosts or two guests may help overcoming these limitations, offering design flexibility. While threads with two pump heads at their extremity have been often employed,[13,15,29] molecules with multiple pendant blue box macrocycles are relatively rare,[30–32] with just one case of a ditopic molecule (**II**·8PF_6, Figure 1b) which was used in combination with nanoparticles, while its redox properties were not investigated.[31] The alkyne-functionalized blue-box **1**·4PF_6 (Figure 2a), of which we recently revisited the synthesis, is ideally suited to prepare analogous ditopic architectures leveraging click chemistry.[26]

In this work, we synthesized two homoditopic structures where either two macrocyclic blue boxes or two viologen units are connected by a poly(ethylene glycol) (PEG) spacer, allowing for systematic electrochemical studies. The analysis revealed an unexpected intramolecular dimerization of ditopic blue-box derivatives, which nevertheless allowed the formation of pseudorotaxanes under reducing conditions. The electrochemical analysis shed light on the kinetics of host-guest interactions, indicating the occurrence of rapid dethreading for most ditopic structures. These findings provide new insights for the development of interlocked polymeric structures.

2 | RESULTS AND DISCUSSION

2.1 | Design and synthesis of homoditopic structures

Building on the optimized synthesis of **1**·4PF_6,[26] we designed homoditopic structures having a PEG spacer linking two functional units: either two macrocycles or two viologens, affording **2**·8PF_6 and **5**·6PF_6, respectively (Figure 2a,b). Their synthesis was achieved via click chemistry: to prepare **2**·8PF_6, **1**·4PF_6 was mixed with an azide-terminating PEG chain (M_w = 1100, comprising ca. 22 repeating units), and Cu(I), in the presence of tris[(1-benzyl-1H-1,2,3-triazol-4-yl)methyl] amine (TBTA). Product formation was confirmed by ^{1}H NMR analysis, as evidenced by the appearance of a characteristic triazole proton signal at ~7.60 ppm, and the deshielding of α- and β-protons adjacent to the triazole ring within the PEG chain (Supporting Information S1: Figures S12 and S13). Product **2**·8PF_6 was isolated in 30% yield after reverse-phase chromatography. Since the crude NMR indicated the presence of product almost exclusively, the modest yield obtained is attributed to the challenging purification. The analog homoditopic structure bearing two terminal viologen units (**5**$^{6+}$, Figure 2b) was prepared using the same approach. To this aim, alkyne-functionalized **4**·3PF_6 (Figure 2b) was first prepared by reacting **3**·2PF_6 with excess 4-bromo-1-butyne (Supporting Information S1: Figures S14 and S15). Then, **4**·3PF_6 was reacted with the azide-terminating PEG precursor used previously. Also in this case, product formation was confirmed by a characteristic triazole peak in the ^{1}H NMR spectrum (Supporting Information S1: Figures S16–S18). The crude mixture was purified twice by reverse-phase chromatography, resulting in a 14% isolated yield. Model monotopic compounds **CBPQT**·4PF_6 (i.e., the blue box) and axle **6**·3PF_6 (Figure 2c) were also prepared and used as references due to their well-established behavior.[10,33] We independently confirmed their redox-controlled self-assembly properties using cyclic voltammetry (CV), differential pulse voltammetry (DPV; Supporting Information S1: Figure S1a,b), and spectroelectrochemistry (SEC, Supporting Information S1: Figure S6).

2.2 | Analysis of individual components

To start with, we investigated the new molecules individually. The CV analysis of **2**·8PF_6 (0.5 mM, Figure 3a) in dry acetonitrile revealed two consecutive redox processes with half-wave potential at −0.29 and −0.72 V. To investigate the reversibility of these processes, CVs were recorded at different scan rates. Both anodic and cathodic peak currents correlate linearly with the square root of the scan rates, with similar slopes, confirming the quasi-reversibility of processes (Supporting Information S1: Figures S4 and S5). These results were corroborated by DPV analysis, which provided values of −0.70 and −0.29 V (Supporting Information S1: Figure S1d), in close agreement with CV data. Thus, CV and DPV analysis indicate that the two macrocycles contained in **2**$^{8+}$ behave similarly.

The species formed upon the first reduction process was also characterized spectroscopically, via SEC analysis. Upon exhaustive reduction (5 min) at −0.5 V, a band at 610 nm appears (Figure 3b). This band is indicative of radical viologen species,[35] and is observed also in the SEC of its similar monotopic counterpart **CBPQT**·4PF_6 (Supporting Information S1: Figure S6).[36] In addition to this band, we also detected a new band around 800 nm, which is not present in

28348966, 0, Downloaded from https://onlinelibrary.wiley.com/doi/10.1002/rpm2.70066 by CochraneItalia, Wiley Online Library on [04/07/2026]. See the Terms and Conditions (https://onlinelibrary.wiley.com/terms-and-conditions) on Wiley Online Library for rules of use; OA articles are governed by the applicable Creative Commons License

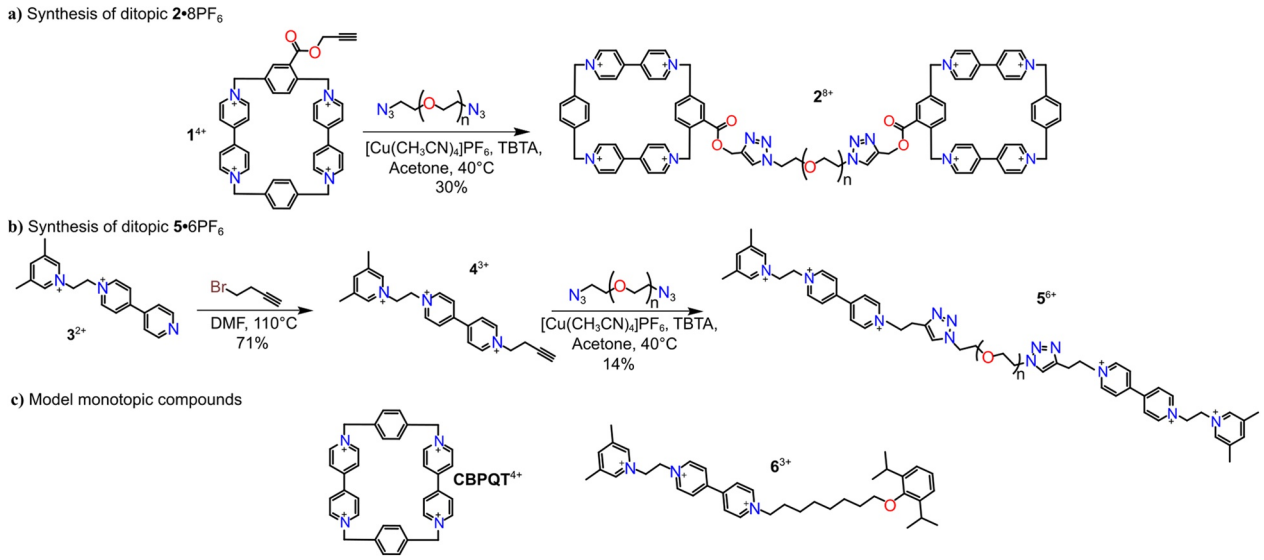


FIGURE 2 Synthetic scheme for the synthesis of (a) **3**·8PF_6 and (b) **4**·6PF_6 via click chemistry. TBTA, tris(benzyltriazolylmethyl)amine. (c) Chemical structures of the model components **CBPQT**·4PF_6 and **6**·3PF_6. *n* ~22.

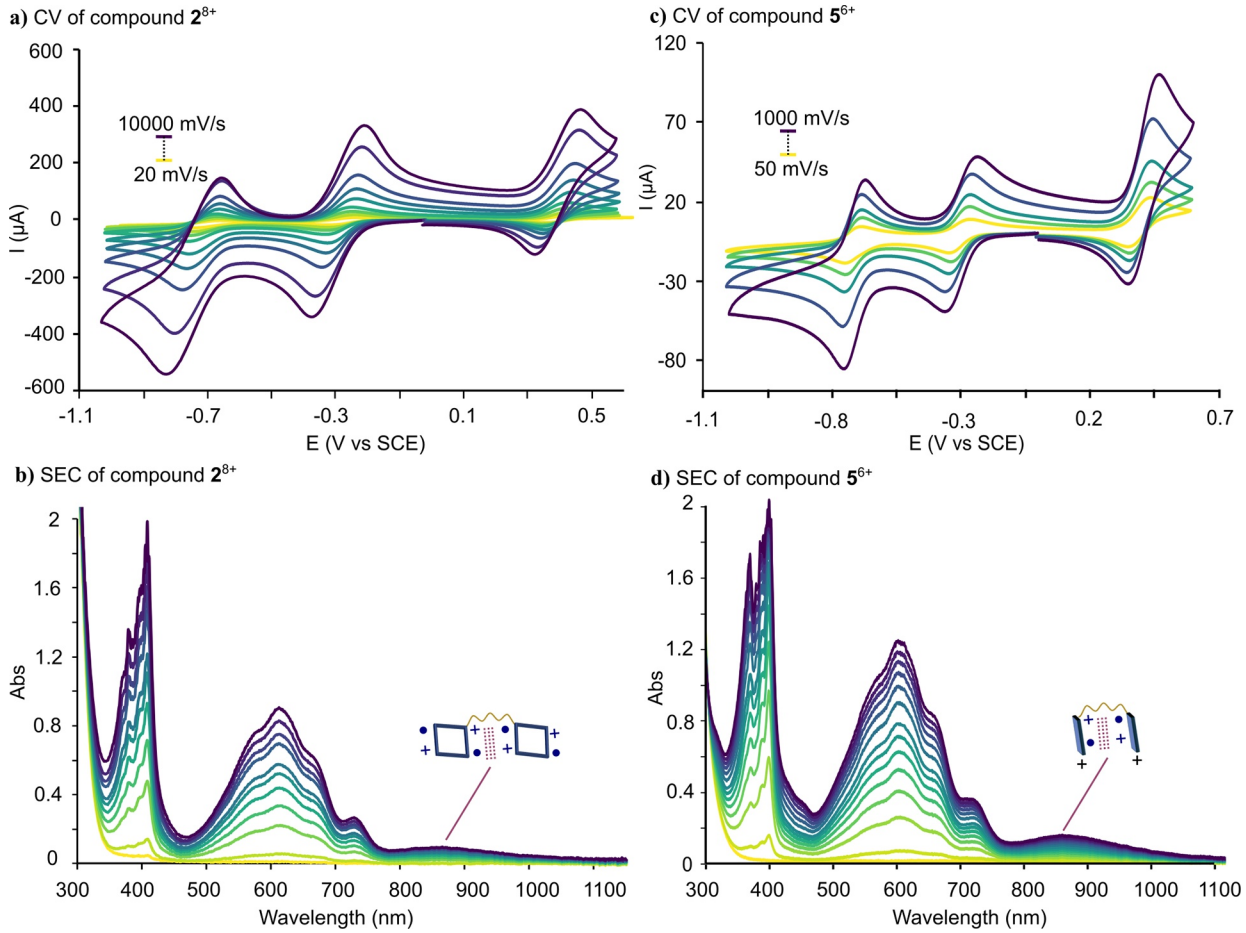


FIGURE 3 (a and b) CV analysis of 0.5 mM of **2**·8PF_6 and **5**·6PF_6 respectively in dry acetonitrile (ACN, 100 mM $TEAPF_6$) at different scan rates. *E* internally referenced to ferrocene (Fc^+/Fc, *E* vs. SCE = 0.395 V).[34] (c and d) Spectroelectrochemistry analysis of 0.5 mM in dry ACN for **2**·8PF_6 and **5**·6PF_6 respectively. The UV-Vis-near IR spectrum was collected during an exhaustive reduction at $E = -0.5$ V for ~5 min. CV, cyclic voltammetry; SEC, spectroelectrochemistry.

28348966, 0, Downloaded from https://onlinelibrary.wiley.com/doi/10.1002/rpm2.70066 by CochraneItalia, Wiley Online Library on [04/07/2026]. See the Terms and Conditions (https://onlinelibrary.wiley.com/terms-and-conditions) on Wiley Online Library for rules of use; OA articles are governed by the applicable Creative Commons License

monotopic **CBPQT**$^{4+}$, indicating the formation of a new species. The presence of two viologen units in the same molecule can lead to the formation of homodimers (intermolecular or intramolecular), characterized by spectroscopic features aligned with our observations.[37,38] The concentration-dependent behavior of the absorption spectrum may help distinguish between intra- and inter-molecular dimerization: since the shape of spectra (Figure 3b, $\lambda > 500$ nm) does not change as the color develops, we tentatively attributed the observed band to the formation of intramolecular homodimers. While homodimerization was observed for molecules that incorporate viologen entities, we are not aware of other reports of homodimerization in structures incorporating blue-box subunits. To assess the generality of this phenomenon, we prepared **II**·8PF$_6$ (Figure 1) and investigated its electrochemical properties (Supporting Information S1: Figures S10 and S11). Also in this case the SEC analysis revealed the formation of a new band at 870–880 nm under reducing conditions, which can be assigned to macrocycle homodimerization.[6,39,40]

The same analysis was performed on compound **5**·6PF$_6$ (Figure 3c). We observed two consecutive redox processes with half-wave potential at −0.31 and −0.72 V. A linear correlation between the peak currents and the square root of the scan rates was obtained for both redox processes (Supporting Information S1: Figures S2 and S3), confirming the quasi-reversible nature of both redox processes. DPV data were in line with CV, affording reduction potentials of −0.71 and −0.28 V (Supporting Information S1: Figure S1c). Also for this ditopic compound, CV and DPV analysis indicate that the two functional units contained in **5**$^{6+}$ behave similarly.

SEC was employed to investigate the possible homodimerization of **5**$^{6+}$. Under reducing conditions, besides the classical band associated with viologen radicals (here at 605 nm), a second band appeared around 865 nm (Figure 3d). The higher apparent absorption coefficient of the homodimer band allowed us to perform concentration-dependent SEC experiments, which showed a linear dependence of absorbance on concentration, as one would expect for an intramolecular process. Based on the acquired data and the spectroscopic information available on structurally related molecules, we interpreted this new band as indicative of a predominantly intramolecular homodimer formation.

Overall, the individual analysis of **2**·8PF$_6$ and **5**·6PF$_6$ indicated that both these ditopic derivatives are electrochemically well-behaved, undergoing quasi-reversible redox processes, and featuring electrochemical properties that resemble those of their monotopic analogs, while presenting a degree of homodimerization upon reduction.

2.3 | Mixture of CBPQT·4PF$_6$ and 6·3PF$_6$—Both monotopic

Having characterized the individual components, we then investigated the self-assembly behavior of all possible combinations of mono and ditopic compounds, to assess the specific effects associated with homoditopicity. We started from the investigation of the model compounds, which were previously investigated, albeit only their bulk reduction and oxidation cycle was presented.[10]

The CV of a 1 mM solution of **CBPQT**·4PF$_6$ and **6**·3PF$_6$ in dry acetonitrile (Figure 4a) can be interpreted on the basis of previous reports,[36,41] and it is useful to illustrate a few key features associated with radical recognition. Despite the fact that two different components are reduced, a single reduction peak is observed at potentials around −0.3 V, both in CV and DPV. This process corresponds to multiple simultaneous reductions which afford the formation of a trisradical tricationic complex, as confirmed by SEC analysis (Figure 4b).[5] Another peculiar feature is the appearance of a reduction process at −0.86 V, which is a value more negative than any process observed for monotopic compounds. This reduction can be tentatively attributed to the reduction of the complex, which occurs at more negative potentials since implies the loss of thermodynamic stabilization initially provided by radical–radical interactions within the complex.[36] A third feature indicative of complex formation is observed in the re-oxidation scan, with a new oxidation wave appearing at 0.005 V. Based on the analysis of similar compounds,[41] we associate the underlying process with the formation of high-energy pseudorotaxane [**6**$^{3+}$ ⊂ **CBPQT**$^{4+}$]. This process occurs at less negative potentials compared to the other processes discussed, because it generates a fully oxidized species, losing the stabilization associated with radical-radical interactions. This process can be observed also in DPV experiments on the same mixture (Supporting Information S1: Figures S7a and S8). Accordingly, a peak at −0.04 V is observed only when performing an oxidative DPV scan, which allows forming the complex in the reduced state before scanning the relevant potential region. When performing a reductive DPV (scanning the potential towards more negative values), no additional peak is detected. Overall, the DPV data are in good agreement with the CV data, being fully consistent with the formation of a high-energy state following re-oxidation, thanks to an energy ratchet mechanism.[42,43]

2.4 | Mixture of 2·8PF$_6$ and 6·3PF$_6$

We increased the level of complexity by replacing monotopic **CBPQT**·4PF$_6$ with ditopic **2**·8PF$_6$. To maintain the same number of viologen units, we mixed 1 mM **6**·3PF$_6$ with 0.5 mM **2**·8PF$_6$, since the latter has twice as much electroactive moieties. The CV shares the key features observed when analyzing monotopic compounds (Figure 4c). At low scan rates it is possible to see both a reduction peak at −0.88 V and a re-oxidation peak at ca. 0.02 V, which are indicative of the formation of radical-radical interactions. At high scan rates, these features become less evident. The DPV analysis (Supporting Information S1: Figures S7b and S8) is mostly consistent with CV data. However, no appreciable peak was observed around 0 V, where the formation of a

28348966, 0, Downloaded from https://onlinelibrary.wiley.com/doi/10.1002/rpm2.70066 by CochraneItalia, Wiley Online Library on [04/07/2026]. See the Terms and Conditions (https://onlinelibrary.wiley.com/terms-and-conditions) on Wiley Online Library for rules of use; OA articles are governed by the applicable Creative Commons License

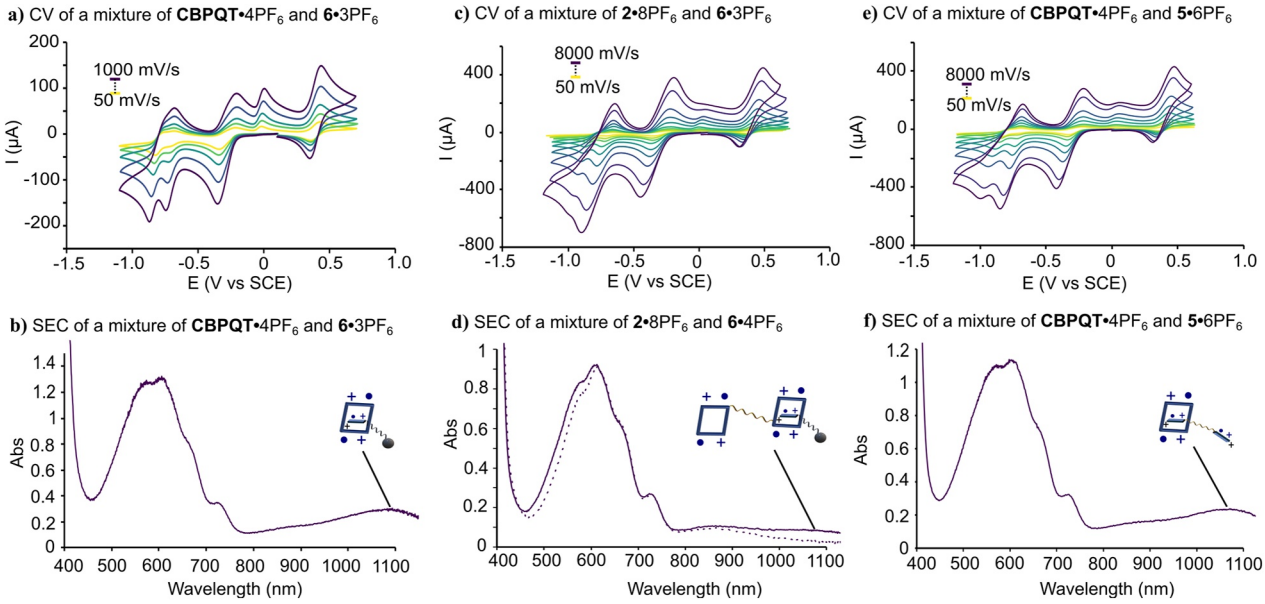


FIGURE 4 Electrochemical analysis of mixture components. (a) CV and (b) SEC of 1 mM **CBPQT**·$4PF_6$ and 1 mM **6**·$3PF_6$. (c) CV and (d) SEC of 0.5 mM **2**·$8PF_6$ and 1 mM **6**·$3PF_6$; the normalized SEC of **2**·$8PF_6$ alone is also reported as dotted line for reference. (e) CV and (f) SEC of 1 mM **CBPQT**·$4PF_6$ and 0.5 mM **5**·$6PF_6$. Conditions: dry ACN (100 mM $TEAPF_6$); *E* internally referenced to ferrocene (Fc^+/Fc, *E* vs. SCE = 0.395 V). CV, cyclic voltammetry; SEC, spectroelectrochemistry.

high-energy state is expected based on model compounds analysis. This observation might be due to a slow association kinetics in the reduced forms $\mathbf{2}^{4(+\cdot)}$ and $\mathbf{6}^{2(+\cdot)}$, or the fast dissociation of the formed inclusion complex. The presence of a DPV peak at −0.78 V (Supporting Information S1: Figures S7b and S8) suggests that an inclusion complex of the type $[\mathbf{6}^{2(+\cdot)} \subset \mathbf{2}^{4(+\cdot)}]$ is indeed forming, a possibility that we investigated using SEC. The appearance of a new band at 1080 nm (Figure 4d) confirms the formation of such species. Two important conclusions are that hetero-radical radical interactions can be established in this system despite the occurrence of intramolecular homo-dimerization, and that the introduction of a PEG chain to connect two macrocyclic moieties is non-innocent, as the dethreading kinetics is impacted.[10] To gain insights on PEG chain role, we performed a control experiment repeating the CV of **CBPQT**·$4PF_6$ and **6**·$3PF_6$ in the presence of an equimolar amount of the azide-terminating PEG chain precursor (Figure 2a). The presence of added PEG did not influence the CV (Supporting Information S1: Figure S7e), implying that PEG cannot act as an intermolecular catalyst for dethreading; the observed effect is thus attributed to an intramolecular effect.

2.5 | Mixture of CBPQT·$4PF_6$ and 5·$6PF_6$

In this case, with respect to the monotopic pair, axle **6**·$3PF_6$ is replaced with ditopic axle **5**·$6PF_6$ while keeping **CBPQT**·$4PF_6$ unchanged. We thus mixed 1 mM **CBPQT**·$4PF_6$ with 0.5 mM **5**·$6PF_6$. The CV (Figure 4e) and DPV data for this pair are qualitatively in line with what observed for the complementary pair formed by monotopic guest **6**·$3PF_6$ and ditopic host **2**·$8PF_6$. Also in this case the DPV (Supporting Information S1: Figures S7c and S8) does not show any additional peak near 0 V, which refers to the presence of the high energy complex. Only a little shoulder appears overlapped with the first reduction peak, at −0.30 V. However, the presence of a peak at −0.79 supports the formation of the inclusion complex $[\mathbf{5}^{2+2(+\cdot)} \subset \mathbf{CBPQT}^{2(+\cdot)}]$. This observation is further validated by SEC where the characteristic inclusion complex band appears at 1080 nm (Figure 4f). An important conclusion provided by the investigation of mono-ditopic mixtures is that the formation of the trisradical trication complex via heterodimerization can be achieved despite the competing intramolecular homodimerization process (Figure 4b,d,f).

2.6 | Mixture of $\mathbf{2}^{8+}$·$8PF_6$ and 5·$6PF_6$—Both ditopic

Having characterized both mono-ditopic pairs, we moved to the investigation of the ditopic-ditopic pair. We thus mixed at 0.5 mM **2**·$8PF_6$ and **5**·$6PF_6$. At a high scan rate (8 V/s) the CV revealed two quasi-reversible processes featuring large peak-to-peak separation (Figure 5a). In contrast with both mono-ditopic pairs, no re-oxidation peak was observed near 0 V in the CV. Accordingly, also the DPV analysis lacked any peak or shoulder near the indicative region, featuring instead three peaks at −0.81, −0.68, and −0.27 V, which appeared consistently in both reductive or oxidative DPV scans (Supporting Information S1: Figures S7d and S8). A possible explanation for the lack of any evidence of high-

28348966, 0, Downloaded from https://onlinelibrary.wiley.com/doi/10.1002/rpm2.70066 by CochraneItalia, Wiley Online Library on [04/07/2026]. See the Terms and Conditions (https://onlinelibrary.wiley.com/terms-and-conditions) on Wiley Online Library for rules of use; OA articles are governed by the applicable Creative Commons License

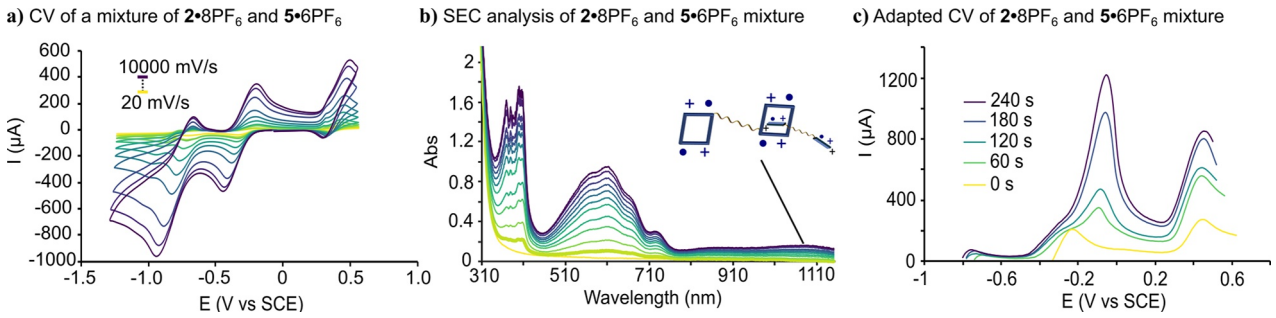


FIGURE 5 Electrochemical analysis of 0.5 mM of both **2**·8PF_6 and **5**·6PF_6 in dry ACN (100 mM $TEAPF_6$). (a) CV of 0.5 mM of **2**·8PF_6 and **5**·6PF_6. (b) SEC of 0.5 mM of **2**·8PF_6 and **5**·6PF_6. UV spectrum was taken during an exhaustive reduction potential of −0.7 V for few minutes. (c) Adapted CV (scan rate = 5 V/s) with incremental time delay (0–240 s). The delay happened at −0.5 V and the oxidation resume its scan in the oxidation direction afterward. *E* internally referenced to ferrocene (Fc^+/Fc, *E* vs. SCE = 0.395 V). CV, cyclic voltammetry; SEC, spectroelectrochemistry.

energy complex formation might be that the complex is not formed at all (scenario 1), or the complex is formed but the macrocycle dethreads quickly (scenario 2).[10,44] The presence of three distinct reduction peaks provides some support for the formation of the trisradical trication complex, but this evidence alone is not sufficient to confirm it.

To exclude the first scenario, we performed SEC analysis, which offered direct evidence of the formation of a trisradical complex. Indeed mixing 0.5 mM of both **2**·8PF_6 and **5**·6PF_6 in dry acetonitrile (ACN) and analyzing them upon exhaustive reduction at −0.5 V revealed the formation of the characteristic radical dimerization band around 1080 nm (Figure 5b).[5] We further corroborated this data by performing a bulk reduction experiment, mixing equimolar amounts of **2**·8PF_6 and **5**·6PF_6 (1.3 mM), and adding activated Zn dust to them. UV-vis-NIR spectroscopy analysis confirmed the formation of characteristic bands at 607, 800, and 1080 nm (Supporting Information S1: Figure S19d). Based on this spectroscopic data, we estimated a 55% yield for complex formation under reducing conditions (see Supporting Information S1: Section 7 for details). Oxidation of this solution afforded the separated individual components.

These observations indicate that under CV, DPV, and bulk redox experiments the disassembly process is faster than the re-oxidation process. To investigate this aspect further, we employed an adapted form of CV, which enabled us to introduce a controlled delay at negative potential (−0.7 to −0.8 V, at which radical-radical interaction are favored thermodynamically) before proceeding with the re-oxidation scan (Supporting Information S1: Figure S9). In such an experiment, by applying a fast scan rate of 5 V/s, we observed the emergence of a new oxidation process at ca. −0.07 V (Figure 5c). The intensity of this new peak increases as the delay time at −0.8 V is extended from 0 to 240 s. Significantly, this additional oxidation wave was not detected when using a scan rate of 0.2 V/s, indicating a strong dependence on the timescale of the electrochemical scan. The absence of the complex at slower scan rates is coherent with the hypothesis that the system has sufficient time to dissociate before detection, whereas faster scans allow the complex to be probed before significant dethreading occurs. Assuming a first-order dethreading process, this behavior suggests a characteristic lifetime between 0.2 and 5 s, since one has to cover about 1 V in between the relevant processes involved, that is, the re-oxidations of the isolated components and the complex. Based on this time window, the apparent rate constant for dethreading would be in the range of 0.2–5 s^{-1}.

Our observations indicate that PEG chains favor rapid dethreading, a conclusion that has some degree of generality since another literature report investigating systems structurally similar to **6**·3PF_6 but containing a short PEG chain (3 or 4 units), reported rapid dethreading after re-oxidation.[10] In our case, the PEG chain is significantly longer and axle **5**·6PF_6 is notably different, as it lacks a bulky stopper. Additionally, **2**·8PF_6 features another PEG chain of similar length, further facilitating fast dethreading. We posit that these combined effects contribute to the rapid relaxation of the high-energy pseudorotaxane to equilibrium. Overall, these data suggest that using a shorter PEG chain in combination with multitopic monomers (rather than ditopic ones) may be helpful to kinetically trap high-energy species within extended networks.

3 | CONCLUSION

In this study, we successfully synthesized and characterized ditopic viologen derivatives, revealing their distinctive electrochemical properties through CV, DPV and SEC, as well as tailored electrochemical sequences. We discovered that both homoditopic compounds (**2**·8PF_6 and **5**·6PF_6) form intramolecular radical homodimers under reducing conditions. We are not aware of previous studies reporting homodimerization of blue box derivatives. Despite the occurrence of intramolecular dimerization, all the investigated host-guest pairs formed pseudorotaxanes thanks to radical-radical interactions. The electrochemical analysis indicated the formation of high-energy states—albeit short-lived—upon cycles of reduction and oxidation. Our findings indicate that PEG spacers influence the kinetics of self-assembly,

28348966, 0, Downloaded from https://onlinelibrary.wiley.com/doi/10.1002/rpm2.70066 by CochraneItalia, Wiley Online Library on [04/07/2026]. See the Terms and Conditions (https://onlinelibrary.wiley.com/terms-and-conditions) on Wiley Online Library for rules of use; OA articles are governed by the applicable Creative Commons License

contributing to variations in redox behavior and leading to rapid disassembly. Overall, this investigation complements previous studies on kinetic aspects of electrochemically-controlled interlocked systems,[45,46] offering new insights into the electrochemical properties of blue box derivatives, as well as fresh guidelines for designing their integration into functional polymeric structures and materials.

4 | EXPERIMENTAL SECTION

4.1 | Synthetic procedures

2·8PF_6. A solution of **1**·4PF_6 (58 mg, 0.013 mmol) and polyoxyethylene bis(azide) (23 mg, 0.021 mmol) in dry acetone (3 mL) was degassed for 20 min followed by the addition of tris[(1-benzyl-1H-1,2,3-triazol-4-yl)methyl]amine (TBTA) (7.14 mg, 0.013 mmol) and $Cu(MeCN)_4PF_6$ (5 mg, 0.049 mmol). The reaction mixture was stirred at 40°C for 2 days, monitoring it by thin layer chromatography using Dragendorff's reagent stain, which revealed the disappearance of PEG starting material. The reaction mixture was concentrated using a rotavapor, resulting in brown crude oil. This oil crude was purified twice via reversed-phase column chromatography (CH_3CN/H_2O = 10:7) to eliminate excess $\mathbf{1}^{4+}$. The fractions containing the product were concentrated by rotary evaporation, obtaining **2**·8PF_6 as a brown solid (14 mg, 30%). ^{19}F NMR was used to confirm and quantify the presence of PF_6^- as counterion. ^{1}H NMR (500 MHz, CD_3CN) δ 9.15–8.87 (m, 16H), 8.50–8.02 (m, 19H), 7.75–7.49 (m, 11H), 6.17 (s, 4H), 5.85 (s, 4H), 5.78 (d, J = 4.1 Hz, 8H), 5.49 (s, 4H), 4.58 (t, J = 4.9 Hz, 3H), 3.91 (t, J = 4.9 Hz, 3H), 3.64–3.47. ^{19}F NMR (376.5 MHz, CD_3CN) δ −71.86 to −73.36. Electrospray ionization - high resolution mass spectrometry (ESI-HRMS) m/z calculated for $[M\text{-}4PF_6]^{4+}$ = 285.843; found m/z = 286.859.

4·3PF_6. A solution of **3**·2PF_6 (400 mg, 0.69 mmol) and 4-bromo but-1-yne (0.914 g, 6.9 mmol) in dry dimethylformamide (8.8 mL) was stirred at 110°C for 3 days. The reaction mixture is then poured into 50 mL of dry acetone. The precipitate is collected, washed with acetonitrile and then dried under vacuum. The solid was then dissolved in minimal amount of water to which a saturated NH_4PF_6 aqueous solution was added until no further precipitation was observed. The precipitate was collected, and washed with water and ether, affording **4**·3PF_6 as a pale-yellow solid (382 mg, 71%). ^{1}H NMR (500 MHz, CD_3CN) δ 8.99–8.95 (m, 2H), 8.82–8.79 (m, 2H), 8.47–8.40 (m, 4H), 8.33 (s, 2H), 8.27 (s, 1H), 5.15 (t, J = 6.5 Hz, 2H), 5.00 (t, J = 6.5 Hz, 2H), 4.78 (t, J = 6.4 Hz, 2H), 2.99 (td, J = 6.4, 2.7 Hz, 2H), 2.49 (s, 6H), 2.46 (t, J = 2.6 Hz, 1H). ^{13}C NMR (126 MHz, CD_3CN) δ 152.75, 151.51, 149.94, 147.56, 147.40, 143.18, 141.49, 129.49, 128.65, 79.29, 75.41, 61.47, 61.42, 60.82, 22.11, 18.90. ESI-HRMS: m/z calculated for $[M\text{-}3PF_6]^{3+}$: 114.737; found: 114.737.

5·6PF_6. A solution of **4**·3PF_6 (180 mg, 0.23 mmol) and polyoxyethylene bis(azide) (101 mg, 0.10 mmol) in dry acetone (8 mL) was degassed for 20 min followed by the addition of tris[(1-benzyl-1H-1,2,3-triazol-4-yl)methyl]amine (TBTA, 33.4 mg, 0.063 mmol) and $Cu(MeCN)_4PF_6$ (23.5 mg, 0.063 mmol). The reaction mixture was stirred at 40°C for 2 days. The reaction mixture was dried under reduced pressure, resulting in a gray solid. This solid was purified twice via reversed-phase column chromatography (CH_3CN/H_2O = 10:7) to eliminate excess $\mathbf{4}^{3+}$. The fractions containing the product were concentrated by rotary evaporation, to afford **5**·6PF_6 as a brown solid (85 mg, 14%). ^{19}F NMR was used to confirm and quantify the presence of PF_6^- as counterion. ^{1}H NMR (500 MHz, CD_3CN) δ 8.87 (th, J = 7.5, 1.7 Hz, 8H), 8.50 (ttq, J = 5.2, 2.7, 1.2 Hz, 4H), 8.42–8.36 (m, 8H), 8.27 (s, 2H), 7.68 (s, 2H), 5.18 (t, J = 6.9 Hz, 4H), 5.01 (dt, J = 13.4, 6.7 Hz, 8H), 4.45 (dd, J = 5.5, 4.6 Hz, 4H), 3.76 (t, J = 5.0 Hz, 4H), 3.58–3.47 (m, 89H), 3.45 (t, J = 6.6 Hz, 4H), 2.49 (s, 12H). ^{13}C NMR (126 MHz, CD_3CN) δ 150.96, 149.83, 147.68, 147.54, 143.32, 142.77, 141.37, 141.37, 141.36, 141.36, 131.27, 131.22, 129.37, 128.41, 125.23, 71.47, 71.46, 71.45, 71.44, 71.43, 71.42, 71.40, 71.39, 71.33, 71.26, 70.32, 62.75, 61.30, 60.77, 51.26, 28.24, 28.22, 18.93. ^{19}F NMR (376.5 MHz, CD_3CN) δ −72.02 to −73.52. ESI-HRMS m/z calculated for $[M\text{-}4PF_6]^{4+}$ = 514.761; found m/z = 514.781.

AUTHOR CONTRIBUTIONS

Ahmad Bachir: Writing—original draft; investigation; methodology; visualization; formal analysis; data curation; conceptualization. **Fabiana Ciocchetti**: Investigation; writing—review and editing; methodology; visualization; formal analysis; data curation; conceptualization. **Caterina Baccini**: Investigation; writing—review and editing; methodology; visualization; formal analysis; data curation. **Sayed Suliman Shah**: Investigation; writing—review and editing. **Andrea Secchi**: Writing—review and editing; validation; supervision; resources; data curation; funding acquisition. **Cristian Pezzato**: Writing—review and editing; validation; data curation. **Giulio Ragazzon**: Resources; supervision; writing—review and editing; validation; data curation; conceptualization; funding acquisition; project administration; writing—original draft.

ACKNOWLEDGMENTS

Georgette Obeid is gratefully acknowledged for preliminary synthetic work. This work was supported by the Interdisciplinary Thematic Institute ITI-CSC via the IdEx Unistra (ANR-10-IDEX-0002) within the program "Investissement d'Avenir", the European Research Council (ERC-2021-StG n. 101041933), and the Italian MIUR (PRIN 20227JMTLE). A. B. thanks the CSC Graduate School funded by the French National Research Agency (CSC-IGS ANR-17-EURE-0016) and the Region Grand Est (ACTION 15 SESRI—Volet 2, 22-DOC-065) for a PhD fellowship.

CONFLICT OF INTEREST STATEMENT

The authors declare no conflicts of interest.

28348966, 0, Downloaded from https://onlinelibrary.wiley.com/doi/10.1002/rpm2.70066 by CochraneItalia, Wiley Online Library on [04/07/2026]. See the Terms and Conditions (https://onlinelibrary.wiley.com/terms-and-conditions) on Wiley Online Library for rules of use; OA articles are governed by the applicable Creative Commons License

DATA AVAILABILITY STATEMENT

The data that supports the findings of this study are available in Supporting Information S1 of this article.

ORCID

Caterina Baccini https://orcid.org/0000-0002-8731-3696
Andrea Secchi https://orcid.org/0000-0003-4045-961X
Cristian Pezzato https://orcid.org/0000-0002-6950-8967
Giulio Ragazzon https://orcid.org/0000-0002-7183-2985

REFERENCES

1. J. F. Stoddart, *Angew. Chem. Int. Ed.* **2017**, *56*, 11094.
2. M. Baroncini, S. Silvi, A. Credi, *Chem. Rev.* **2020**, *120*, 200.
3. B. Odell, M. V. Reddington, A. M. Z. Slawin, N. Spencer, J. F. Stoddart, D. J. Williams, *Angew. Chem. Int. Ed.* **1988**, *27*, 1547.
4. X. Y. Chen, H. Chen, J. Fraser Stoddart, *Angew. Chem. Int. Ed.* **2023**, *62*, e202211387.
5. A. Trabolsi, N. Khashab, A. C. Fahrenbach, D. C. Friedman, M. T. Colvin, K. K. Cotí, D. Benítez, E. Tkatchouk, J.-C. Olsen, M. E. Belowich, R. Carmielli, H. A. Khatib, W. A. Goddard, M. R. Wasielewski, J. F. Stoddart, *Nat. Chem.* **2010**, *2*, 42.
6. C. K. Lee, C. Gangadharappa, A. C. Fahrenbach, D. J. Kim, *Adv. Mater.* **2024**, *36*, 2408271.
7. J. Joseph, M. Berville, J. Wytko, J. Weiss, H. P. Jacquot de Rouville, *Chem. Eur. J.* **2025**, *31*, e202403115.
8. K. Cai, L. Zhang, R. D. Astumian, J. F. Stoddart, *Nat. Rev. Chem.* **2021**, *5*, 447.
9. J. M. Spruell, W. F. Paxton, J. Olsen, D. Benitez, E. Tkatchouk, C. L. Stern, A. Trabolsi, D. C. Friedman, W. A. Goddard, J. F. Stoddart, *J. Am. Chem. Soc.* **2009**, *131*, 11571.
10. C. Cheng, P. R. McGonigal, W. G. Liu, H. Li, N. A. Vermeulen, C. Ke, M. Frasconi, C. L. Stern, W. A. Goddard, J. F. Stoddart, *J. Am. Chem. Soc.* **2014**, *136*, 14702.
11. C. Cheng, P. R. McGonigal, S. T. Schneebeli, H. Li, N. A. Vermeulen, C. Ke, J. F. Stoddart, *Nat. Nanotechnol.* **2015**, *10*, 547.
12. C. Pezzato, M. T. Nguyen, C. Cheng, D. J. Kim, M. T. Otley, J. F. Stoddart, *Tetrahedron* **2017**, *73*, 4849.
13. C. Pezzato, M. T. Nguyen, D. J. Kim, O. Anamimoghadam, L. Mosca, J. F. Stoddart, *Angew. Chem. Int. Ed.* **2018**, *57*, 9325.
14. Y. Qiu, L. Zhang, C. Pezzato, Y. Feng, W. Li, M. T. Nguyen, C. Cheng, D. Shen, Q. H. Guo, Y. Shi, K. Cai, F. M. Alsubaie, R. D. Astumian, J. F. Stoddart, *J. Am. Chem. Soc.* **2019**, *141*, 17472.
15. Y. Qiu, B. Song, C. Pezzato, D. Shen, W. Liu, L. Zhang, Y. Feng, Q. H. Guo, K. Cai, W. Li, H. Chen, M. T. Nguyen, Y. Shi, C. Cheng, R. D. Astumian, X. Li, J. F. Stoddart, *Science* **2020**, *368*, 1247.
16. L. Feng, Y. Qiu, Q.-H. Guo, Z. Chen, J. S. W. Seale, K. He, H. Wu, Y. Feng, O. K. Farha, R. D. Astumian, J. F. Stoddart, *Science* **2021**, *374*, 1215.
17. C. K. Lee, Y. Feng, A. E. Enciso, J. P. Violi, W. A. Donald, J. F. Stoddart, D. J. Kim, *Chem* **2025**, *12*, 102693.
18. J. S. W. Seale, S. Sharma, C. K. Lee, H. Han, T. Jaynes, E. W. Roth, S. Shafie, Y. Qiu, L. Malaisrie, M. I. Bardot, L. Zhang, Y.-K. Xing, D. J. Kim, S. I. Stupp, R. D. Astumian, E. A. Scott, W. R. Dichtel, J. F. Stoddart, *Angew. Chem. Int. Ed.* **2025**, *137*, e202512899.
19. C. K. Lee, J. P. Violi, W. A. Donald, J. F. Stoddart, D. J. Kim, *Nat. Commun.* **2025**, *16*, 5922.
20. C. J. Bruns, M. Frasconi, J. Iehl, K. J. Hartlieb, S. T. Schneebeli, C. Cheng, S. I. Stupp, J. F. Stoddart, *J. Am. Chem. Soc.* **2014**, *136*, 4714.
21. K. Cai, B. Cui, B. Song, H. Wang, Y. Qiu, L. O. Jones, W. Liu, Y. Shi, S. Vemuri, D. Shen, T. Jiao, L. Zhang, H. Wu, H. Chen, Y. Jiao, Y. Wang, C. L. Stern, H. Li, G. C. Schatz, X. Li, J. F. Stoddart, *Chem* **2021**, *7*, 174.
22. A. C. Benniston, A. Harriman, *Synlett* **1993**, *3*, 223.
23. A. B. Braunschweig, W. R. Dichtel, O. Š. Miljanić, M. A. Olson, J. M. Spruell, S. I. Khan, J. R. Heath, J. F. Stoddart, *Chem. Asian J.* **2007**, *2*, 634.
24. M. A. Olson, A. B. Braunschweig, T. Ikeda, L. Fang, A. Trabolsi, A. M. Z. Slawin, S. I. Khan, J. F. Stoddart, *Org. Biomol. Chem.* **2009**, *7*, 4391.
25. M. P. L. Werts, M. van den Boogaard, G. M. Tsivgoulis, G. Hadziioannou, *Macromolecules* **2003**, *36*, 7004.
26. A. Bachir, F. Ciocchetti, D. P. Couto, S. Di Noja, C. Pezzato, G. Ragazzon, *Eur. J. Org. Chem.* **2023**, *26*, e202300498.
27. K. Cai, Y. Shi, G. Zhuang, L. Zhang, Y. Qiu, D. Shen, H. Chen, Y. Jiao, H. Wu, C. Cheng, J. F. Stoddart, *J. Am. Chem. Soc.* **2020**, *142*, 10308.
28. C. K. Lee, Y. Feng, M. Tajik, J. P. Violi, W. A. Donald, J. F. Stoddart, D. J. Kim, *J. Am. Chem. Soc.* **2024**, *146*, 27109.
29. J. S. W. Seale, B. Song, Y. Qiu, J. F. Stoddart, *J. Am. Chem. Soc.* **2022**, *144*, 16898.
30. R. Klajn, M. A. Olson, P. J. Wesson, L. Fang, A. Coskun, A. Trabolsi, S. Soh, J. F. Stoddart, B. A. Grzybowski, *Nat. Chem.* **2009**, *1*, 733.
31. M. A. Olson, A. Coskun, R. Klajn, L. Fang, S. K. Dey, K. P. Browne, B. A. Grzybowski, J. F. Stoddart, *Nano Lett.* **2009**, *9*, 3185.
32. M. Bria, J. Bigot, G. Cooke, J. Lyskawa, G. Rabani, V. M. Rotello, P. Woisel, *Tetrahedron* **2009**, *65*, 400.
33. P. L. Anelli, P. R. Ashton, R. Ballardini, V. Balzani, M. Delgado, M. T. Gandolfi, T. T. Goodnow, A. E. Kaifer, D. Philp, *J. Am. Chem. Soc.* **1992**, *114*, 193.
34. G. Ragazzon, C. Schäfer, P. Franchi, S. Silvi, B. Colasson, M. Lucarini, A. Credi, *Proc. Natl. Acad. Sci. U. S. A.* **2018**, *115*, 9385.
35. C. Lee, Y. M. Lee, M. S. Moon, S. H. Park, J. W. Park, K. G. Kim, S. J. Jeon, *J. Electroanal. Chem.* **1996**, *416*, 139.
36. Y. Jiao, Y. Qiu, L. Zhang, W. G. Liu, H. Mao, H. Chen, Y. Feng, K. Cai, D. Shen, B. Song, X. Y. Chen, X. Li, X. Zhao, R. M. Young, C. L. Stern, M. R. Wasielewski, R. D. Astumian, W. A. Goddard, J. F. Stoddart, *Nature* **2022**, *603*, 265.
37. C. M. Ronconi, J. F. Stoddart, V. Balzani, M. Baroncini, P. Ceroni, C. Giansante, M. Venturi, *Chem. Eur. J.* **2008**, *14*, 8365.
38. K. Wadhwa, S. Nuryyeva, A. C. Fahrenbach, M. Elhabiri, C. Platas-Iglesias, A. Trabolsi, *J. Mater. Chem. C* **2013**, *1*, 2302.
39. K. Madasamy, M. Kathiresan, *ChemistrySelect* **2016**, *1*, 354.
40. S. Al Shehimy, O. Baydoun, S. Denis-Quanquin, J. C. Mulatier, L. Khrouz, D. Frath, É. Dumont, M. Murugesu, F. Chevallier, C. Bucher, *J. Am. Chem. Soc.* **2022**, *144*, 17955.
41. C. Cheng, T. Cheng, H. Xiao, M. D. Krzyaniak, Y. Wang, P. R. McGonigal, M. Frasconi, J. C. Barnes, A. C. Fahrenbach, M. R. Wasielewski, W. A. Goddard, J. F. Stoddart, *J. Am. Chem. Soc.* **2016**, *138*, 8288.
42. T. Sangchai, S. Al Shehimy, E. Penocchio, G. Ragazzon, *Angew. Chem. Int. Ed.* **2023**, *62*, e202309501.
43. S. Borsley, B. M. W. Roberts, D. A. Leigh, *Angew. Chem. Int. Ed.* **2024**, *63*, e202400495.
44. Z. Zhu, H. Li, Z. Liu, J. Lei, H. Zhang, Y. Y. Botros, C. L. Stern, A. A. Sarjeant, J. F. Stoddart, H. M. Colquhoun, *Angew. Chem. Int. Ed.* **2012**, *51*, 7231.
45. S. S. Andersen, A. W. Saad, R. Kristensen, T. S. Pedersen, L. J. O. Driscoll, A. H. Flood, J. O. Jeppesen, *Org. Biomol. Chem.* **2019**, *17*, 2432.
46. M. S. Neumann, S. K. Jensen, R. Frederiksen, S. S. Andersen, K. M. Becka, J. O. Jeppesen, *Org. Biomol. Chem.* **2024**, *22*, 9203.

SUPPORTING INFORMATION

Additional supporting information can be found online in the Supporting Information section at the end of this article.

How to cite this article: A. Bachir, F. Ciocchetti, C. Baccini, S. S. Shah, A. Secchi, C. Pezzato, G. Ragazzon, *Responsive Mater.* **2026**, e70066. https://doi.org/10.1002/rpm2.70066

28348966, 0, Downloaded from https://onlinelibrary.wiley.com/doi/10.1002/rpm2.70066 by CochraneItalia, Wiley Online Library on [04/07/2026]. See the Terms and Conditions (https://onlinelibrary.wiley.com/terms-and-conditions) on Wiley Online Library for rules of use; OA articles are governed by the applicable Creative Commons License